ORIGINAL RESEARCH

Acute hematologic, hepatologic, and nephrologic changes after intraperitoneal injections of 18 nm gold nanoparticles in hamsters

Hazem Mohamed Saleh[1]
Omar A Soliman[2]
Mohamed Osama Elshazly[3]
Alaa Raafat[2]
Adel K Gohar[2]
Taher A Salaheldin[4]

[1]Otolaryngology Unit, Department of Medical Applications, The National Institute of Laser Enhanced Sciences, Cairo University, [2]Department of Clinical Pathology, [3]Department of Pathology, Faculty of Veterinary Medicine, Cairo University, [4]Nanotechnology & Advanced Materials Central Laboratory, Agricultural Research Center, Guiza, Egypt

Correspondence: Hazem Mohamed Saleh
Otolaryngology Unit, Department of Medical Applications, The National Institute of Laser Enhanced Sciences, Cairo University, 10 El Messaha Square, Apartment 1401, 12311 Guiza, Egypt
Tel +20 2 3748 2838
Email hazemsalehniles@yahoo.com

Abstract: In vivo responses to gold nanoparticles (GNPs) vary not only according to the size, shape, surface charge, and capping agent of GNPs but also according to the animal model, the route of administration, and the exposure frequency and duration. We illustrate here the changes in some hematologic parameters, in the hepatic and renal functions, and in the histopathology of solid organs after multiple intraperitoneal injections of 18 nm GNPs in adult male Syrian golden hamsters. We scored the histopathological changes in the liver and kidneys to grade the deleterious effects. Multiple intraperitoneal injections of 18 nm GNPs in hamsters were nonlethal in the short term but resulted in macrocytosis and hypochromasia, leukocytosis, neutrophilia, lymphocytosis, and monocytosis. The hepatic and renal functions showed nonsignificant changes; however, histopathological examination showed hepatic and renal alterations ranging from mild to marked degeneration, with occasional necrosis of hepatocytes and tubular epithelium.

Keywords: in vivo, hamsters, nanogold, acute

Background

Materials at the nanoscale (1–100 nm) differ from their larger counterparts in being more reactive due to a relatively large surface-to-diameter ratio. Gold nanoparticles (GNPs) have unique physical and chemical properties, such as biocompatibility and ease of preparation and modification,[1,2] and unique optical properties arising from the surface plasmon oscillation of free electrons.[3] GNP properties are convenient for biomedical applications, such as drug and gene delivery,[4,5] DNA detection,[6] bioimaging,[7–9] and photothermal therapy of cancers.[10,11]

GNP safety data derived from studies on tissue cultures may not reflect the real picture in vivo.[12] Available in vivo data are contradictory. Many reports concluded that GNPs do not produce toxicity in laboratory animals.[13–15] Others claimed that GNPs induce morbidity and mortality when injected in the same animals.[16] GNP-induced changes are attributed to their sizes able to cross the biological barriers.[17–19] The particle surface chemistry and charge also have important roles in the induced changes due to their immunogenicity and effects on bioclearance.[13,15,20–24] The route of administration has a major impact on GNP-induced effects. Intravenous route was shown to be the safest[12,25] followed by subcutaneous application.[24] On the other hand, intraperitoneal (I/P) administration of GNPs showed a moderate toxicity,[12,16] while the oral route was the most toxic.[12,26]

Eighteen-nanometer GNPs were found to have a high retention rate in living organisms after intraesophageal administration with a high accumulation rate in solid organs,

such as the brain and heart.[27] It was hypothesized that the specific curvature and surface structure of the 18 nm GNPs alter the structure and function of single adsorbed proteins or select proteins, increasing the probability of intestinal epithelial penetration for the 18 nm GNPs compared to other GNP sizes. Also, 24 hours after intravenous injection in mice, 18 nm GNPs showed a high retention in blood cells compared to serum, indicating their partial binding to blood cells. It showed indeed >90% accumulation in the liver. Single 18 nm GNPs were found in hepatocytes and endothelial cells indicating little agglomeration in the blood.[28]

Syrian golden hamsters (*Mesocricetus auratus*) are widely used to model cancers, especially cancers of the upper aerodigestive tract.[29] The pattern of the upper aerodigestive tree, and esophageal cancers produced in hamsters resembles that seen in human smokers and suggests that this model may serve as a system for testing chemopreventive or chemotherapeutic agents for tumors in these areas.[30]

As far as we know, no quantitative or semiquantitative biodistribution study of the 18 nm GNPs after in vivo I/P administration in hamsters exists. Thereby, the aim of this study was to investigate the effects of repeated I/P injection of 18 nm sized GNPs on some hematologic parameters, on the hepatic and renal functions and on the histopathology of solid organs in healthy adult male Syrian golden hamsters receiving 30 ppb of GNPs daily for 14 consecutive days (a total dose of 420 ppb per animal). The observed effects were assessed in a semiquantitative manner to serve as a baseline, where the effects of intralesional administrations of GNPs in a hamster tumor model that we developed are compared with those of systemic injections of GNPs in the same model. This work is part of a project aiming to assess the safety and efficacy of GNPs in the diagnosis and photothermal therapy of chemically induced oral cancers.

Materials and methods
GNPs' preparation and characterization

GNPs were prepared by citrate reduction of gold(III) chloride trihydrate following the Frens modification of the Turkevich method.[31] Before the reduction process, all glassware was cleaned in aqua regia (three parts HCl and one part HNO_3), rinsed with deionized H_2O, and then dried. An aqueous solution of gold(III) chloride trihydrate ($\geq$99.9%; Sigma-Aldrich Co., St Louis, MO, USA) was brought to boiling and stirred continuously. A solution of 38.8 mM sodium citrate tribasic dehydrate ($\geq$98%; Sigma-Aldrich Co.) was added quickly, resulting in a change in solution color from pale yellow to black to deep red. A 50:2 ratio of tetrachloroauric acid to

citrate was used in order to obtain the particles of ~18 nm size. GNPs were washed three times with deionized water to remove the nonreacted precursors. The prepared nanoparticles were then characterized using the ultraviolet-visible (UV-Vis) absorption spectrophotometer (Cary 5000; Agilent, Santa Clara, CA, USA), the particle size analyzer (Malvern Zetasizer Nano ZSPXRD; Malvern Instruments, Malvern, UK), and the transmission electron microscopy (TEM) (Tecnai; FEI, Eindhoven, the Netherlands). Absorption spectra were recorded using a double beam UV-Vis spectrophotometer. The absorption spectra of the diluted solutions of prepared GNPs in aqueous medium were recorded within the appropriate scan range (400–850 nm). The spectrum of the pure solvent was taken as a calibrating reference. Measurements were performed at room temperature. The morphology of GNPs and their particle sizes were examined under TEM operating at an accelerating voltage of 80 kV. A drop from a dilute sample solution was deposited on an amorphous carbon-coated copper grid and left to evaporate at room temperature forming a monolayer. Analysis of the particle size diameters of prepared GNPs was estimated using the software program Gaten over several shots of TEM images for the target sample. The purity of GNPs was assessed by energy-dispersive X-ray spectroscopy on TEM. In order to calculate the volume to be injected in each animal, the concentration of gold in solution was determined by atomic absorption spectroscopy (SpectrAA 220; Varian Medical Systems).

In vivo animal experiments

A total of 20 adult male Syrian golden hamsters were purchased from the Holding Company for Biological Products and Vaccines (VACSERA), Helwan, Cairo, Egypt. The hamsters were of nearly uniform age (10–12 weeks) and weight (100–150 g). The animal care protocol was in compliance with the Humane Care for Animals Act, the guidelines of The Canadian Council of Animal Care, and the EU Directive 2010/63/EU for animal experiments. The study design was approved by the Animal Care Committee at the Faculty of Veterinary Medicine, Cairo University, Egypt. Hamsters were fed on dry, 26% protein pellets and tap water ad libitum. They were housed two to three hamsters per cage in a temperature-controlled and well-ventilated breeding area in a 12-hour light/dark cycle. The environmental conditions were monitored twice daily. Hamsters were kept under observation for 2 weeks before starting the experiment to ensure full conditioning and healthy state. They were randomly divided into two groups: the control group, consisting of ten hamsters, kept under

similar environmental conditions to the injected group, also consisting of ten animals. In the injected group, each animal received one I/P injection of 0.5 mL of GNPs (30 ppb) daily for 14 consecutive days. At the end of the experiment, animals were anesthetized diethyl ether (SD Fine-Chem Ltd, Chennai, India). Blood was collected from the retro-orbital venous plexus in tubes containing disodium ethylene diamine tetra-acetic acid (El Nasr Pharmaceutical Chemicals Company, ADWIC, Nasr Pharma, Qalyub, Egypt) for complete blood count and in plain vacutainers to yield serum by centrifugation (3,000 rpm for 10 minutes). Serum was kept at −20°C for biochemical tests. Animals were euthanized by intracardiac injection of overdose of Mepacaine L (each 1 mL contains mepivacaine HCl 20.0 mg and levonordefin HCl 0.06 mg; Alexandria Co., Pharmaceuticals, Alexandria, Egypt). Solid organs were dissected and taken for histopathological examination.

Complete blood count

Red blood cell (RBC) and white blood cell counts were performed using an improved Neubauer hemocytometer. Packed cell volume was estimated by the microhematocrit technique. Hemoglobin concentration was determined colorimetrically using the cyanmethemoglobin method. Differential leukocytic count was performed on the stained blood smear according to Feldman et al.[32]

Biochemical tests

Hepatic and renal function tests were measured using diagnostic kits (Spectrum Diagnostics, Obour City, Egypt) according to the manufacturer's recommendations. Total proteins were measured as described by Weichselbaum,[33] albumin was measured as described by Dumas and Biggs,[34] ALT and AST were measured as described by Reitman and Frankel,[35] urea was measured as described by Searcy et al,[36] and creatinine was measured as described by Fabiny and Ertingshausen.[37]

Tissue distribution

Tissue distribution was assessed by flame atomic absorption spectroscopy (SpectrAA 220; Varian Medical Systems). Tissue samples were prepared according to Kehoe et al[38] where known amounts of tissues are weighed and digested by a mixture of perchloric and nitric acid (1:3) while heating at 200°C.

Statistical analysis of the biochemical tests

Data were presented as mean ± SD. Independent samples Student's t-test was used to compare mean between groups after assuring normal distribution of the data using Shapiro–Wilk test. The significance level was set as P-value ≤0.05. Statistical analysis was performed using the SPSS software version 16.

Histopathological examination

After taking the blood samples and euthanizing the laboratory animals from both groups, the liver, kidneys, spleen, and lungs were carefully dissected and collected as whole organ specimens from all experimental animals. Organs were fixed in neutral buffered formalin (10%) then dehydrated, with sequential exposure to grades of ethanol (70%, 80%, 90%, 95%, and 100%). Dehydration was followed by clearing the samples in two changes of Xylene. Samples were impregnated with two changes of molten paraffin wax, then embedded, and blocked out. Paraffin sections of 5 µm thickness were cut using a rotatory microtome (Leica RM 2235, Leica Biosystems, Nussloch, Germany), stained with hematoxylin and eosin according to Bancroft et al,[39] and examined using an optical microscope (Olympus BX 50; Olympus Corporation, Tokyo, Japan). Histopathological diagnosis was performed according to the Standardized System of Nomenclature and Diagnostic Criteria.[40]

Scoring system

Semiquantitative scoring to determine the extent of injury in the liver and kidneys was done using a four-digit numerical scoring system where 0 indicates no change and 1–4 indicate increasing severity according to Mann et al.[41]

Statistical analysis of the scoring

The obtained scores were presented as mean ± standard deviation. Statistical significance between the different groups was analyzed using the analysis of variance test (SPSS 10.0) followed by Duncan's multiple range test.[42]

Results
GNP characterization

The prepared GNPs showed a maximum extinction of 1.228 at 535 nm by UV-Vis spectrophotometer (Figure 1A). TEM images showed that the examined particles (n=100) have a spherical shape with a mean particle diameter of 18 nm (±1.1 nm) (Figure 1B). Particle size distribution assessed by zetasizer showed peak percentage (22.9%) at 18 nm diameter (Figure 1C). The energy-dispersive X-ray spectroscopy showed peaks corresponding to Au element at 2.12 keV, 9.44 keV, and 11.4 keV, confirming the existence of GNPs. In addition, acceptable peaks for C at 0.277 keV
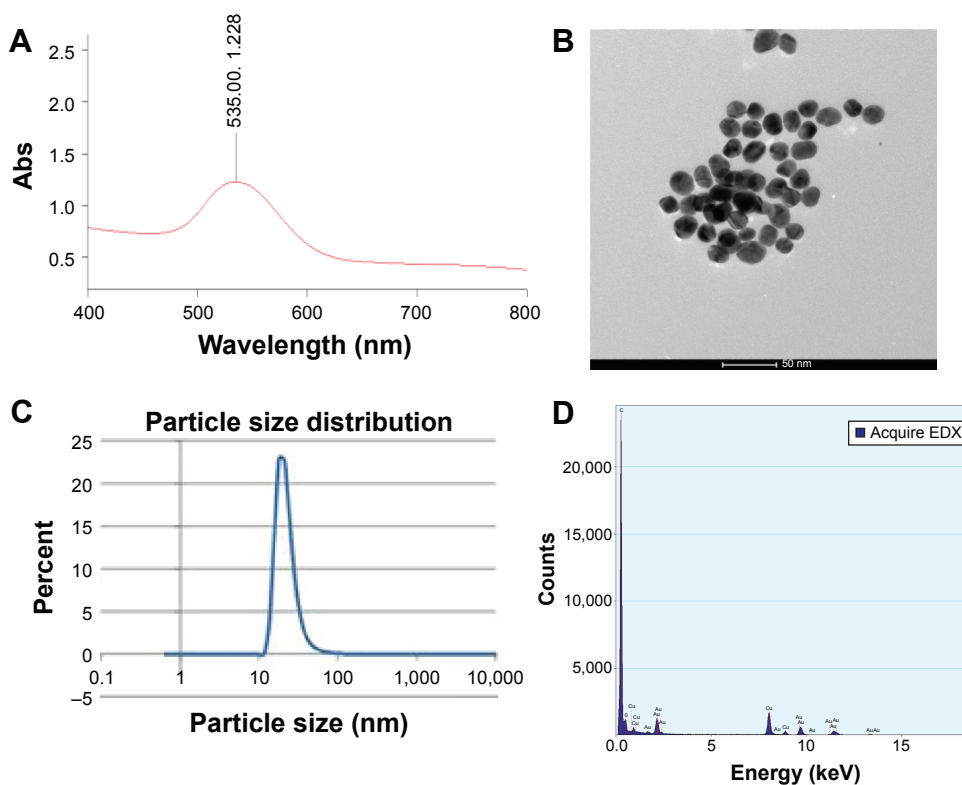
Figure 1 GNPs characterization.
Notes: (**A**) Peak absorption of prepared GNPs (1.2) at 535 nm wavelength. (**B**) TEM images showing gold nanospheres with average 18 nm diameter (magnification, 97,000×). (**C**) Particle size distribution by zeta sizer showing peak percent (22.9%) at 18 nm diameter. (**D**) EDX showing peaks corresponding to Au element at 2.12 keV, 9.44 keV, and 11.4 keV, confirming the existence of GNPs.
Abbreviations: EDX, energy-dispersive X-ray spectroscopy; GNPs, gold nanoparticles; TEM, transmission electron microscopy; Abs, absorbance.

and for Cu at 0.93 keV, 8.04 keV, and 8.9 keV were observed owing to the composition of copper grid used in the TEM imaging process (Figure 1D).

Clinical signs

No hamster mortality occurred during the 14 days of I/P injection of GNPs. Furthermore, no abnormal clinical signs or behaviors were detected in the injected or in the control groups. No changes were noticed in the fur, and there was no discharge. Necropsy at the end of the experiment did not show any macroscopic changes in the organs of the injected group.

Erythrogram

Results of the erythrogram showed significantly higher mean packed cell volume and mean corpuscular volume in the injected group ($P \leq 0.05$). On the other hand, the mean cell hemoglobin concentration in the injected group was significantly lower than in the control group as shown in Table 1.

Leukogram

Leukocytosis was evident in hamsters of the injected group. Neutrophilia, lymphocytosis, and monocytosis occurred.

On the contrary, no difference was noticed in the eosinophil and basophil counts between the injected and control groups. Results of the leukogram are shown in Table 1.

Liver function tests

None of the assessed parameters (total proteins, albumin, globulin, albumin/globulin ratio, ALT, and AST) showed statistically significant differences between the injected and control groups as shown in Table 1.

Kidney function tests

There was no statistically significant difference in the mean values of urea and creatinine levels in serum between the injected and control groups as shown in Table 1.

Tissue distribution

Results of tissue distribution demonstrated that, in the GNP-injected hamsters, gold accumulated mainly in the liver (7.85±0.55 μg Au/g tissue) followed by the spleen (6.47±0.54 μg/g) and heart (6.37±0.58 μg/g). Pulmonary and renal tissues showed less concentration of gold (4.02±0.64 μg/g and 3.74±0.46 μg/g, respectively). On the other hand, tissues of control animals showed absence of any residue of gold as illustrated in Table 1.

Table 1 Mean ± SD of clinical hematology, clinical chemistry, and tissue distribution data

Parameter	Control	Injected
Erythrogram		
PCV (%)	29.50±1.29	35.33±3.21*
Hb (g/dL)	8.63±0.92	7.90±0.36
RBCs count (×10⁶ cell/µL)	5.55±0.84	4.50±0.26
MCV (fL)	53.89±6.78	78.99±12.15*
MCH (pg)	15.77±2.56	17.62±1.79
Leukogram (10³ cell/µL)		
TLC	0.50±0.14	1.83±0.28*
Neutrophil	0.50±0.14	1.83±0.28*
Lymphocyte	2.19±0.18	2.58±0.15*
Monocyte	0.01±0.03	0.72±0.20*
Eosinophil	0.00±0.00	0.00±0.00
Basophil	0.00±0.00	0.00±0.00
Liver function		
Total protein (g/dL)	6.07±0.15	6.52±0.73
Albumin (g/dL)	3.37±0.06	3.53±0.51
Globulin (g/dL)	2.34±0.12	3.00±0.86
A/G ratio	1.60±0.08	1.29±0.52
ALT (U/L)	72.00±8.66	74.40±8.85
AST (U/L)	30.00±6.56	39.20±6.02
Renal function		
Urea (mg/dL)	51.13±5.32	51.91±6.61
Creatinine (mg/dL)	0.66±0.13	0.76±0.10
Gold residues (µg/g)		
Liver	0.00±0.00	7.85±0.55*
Spleen	0.00±0.00	6.47±0.54*
Heart	0.00±0.00	6.37±0.58*
Lung	0.00±0.00	4.02±0.64*
Kidney	0.00±0.00	3.74±0.46*

Notes: Values represent mean ± SD. *Significant difference at *P*-value ≤0.05.
Abbreviations: A/G, albumin/globulin; Hb, hemoglobin; MCV, mean corpuscular volume; PCV, packed cell volume; RBCs, red blood cells; TLC, total leukocyte count; AST, aspartate aminotransferase; ALT, alanine aminotransferase; MCH, mean corpuscular hemoglobin.

Histopathological examination

Histopathological examination of different organs, namely the liver, kidneys, lungs, heart, and spleen, from animals of the control group did not reveal any structural abnormality. Hamsters of the injected group showed normal structure of the spleen, lungs, and heart except for mild-to-moderate congestion of blood vessels, whereas hepatic and renal tissues showed variable histopathological alterations of varying severity and extent as follows:

Liver

Mild-to-moderate and marked focal and diffuse vacuolar degeneration of hepatocytes together with Kupffer cell hyperplasia/upregulation and congestion of the central and portal blood vessels were commonly observed in almost all cases (Figure 2A). Mild-to-moderate perivascular and portal monolymphocytic cell infiltration (Figure 2B) and variable sized sporadic foci of hepatic necrosis scattered throughout the hepatic parenchyma along with replacement of the necrotic tissue with mononuclear cells were commonly seen (Figure 2C). Occasional paracentral areas of coagulative necrosis of hepatocytes with mononuclear cell infiltration (Figure 2D) and/or foci of coagulative necrosis of hepatocytes associated with sinusoidal leukocytosis (Figure 2E) were also observed.
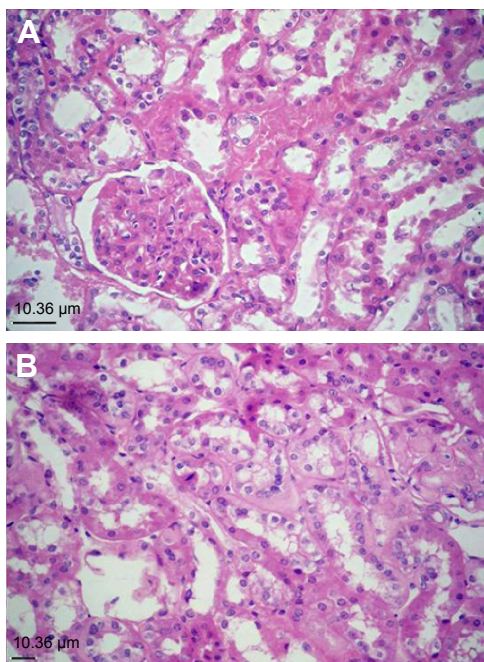
Kidneys

Renal cortex in almost all hamsters of the injected group revealed vacuolar degeneration and necrosis of tubular
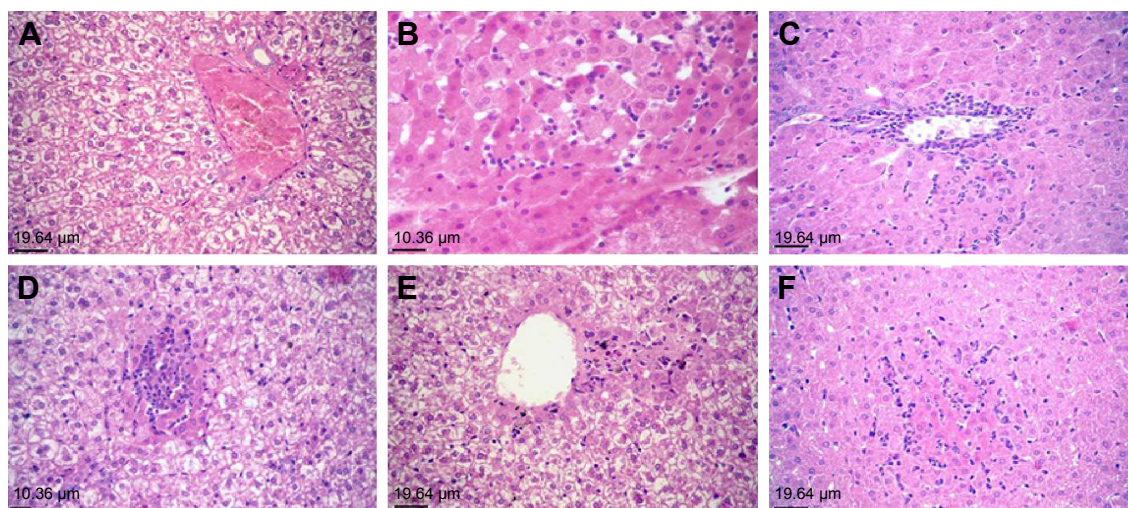
Figure 2 Liver and kidneys of hamsters of the injected group.
Notes: (**A**) Liver of a hamster of the injected group showing marked vacuolar degeneration of hepatocytes and congestion of hepatic blood vessels (hematoxylin and eosin stain [H&E], magnification, ×20). (**B**) Liver of a hamster of the injected group showing perivascular mononuclear cell infiltration (H&E, ×20). (**C**) Liver of a hamster of the injected group showing sporadic foci of hepatic necrosis scattered throughout the hepatic parenchyma along with replacement of the necrotic tissue with mononuclear cells (H&E, ×20). (**D**) Liver of a hamster of the injected group showing paracentral area of coagulative necrosis of hepatocytes with mononuclear cell infiltration (H&E, ×20). (**E**) Liver of a hamster of the injected group showing focal areas of hepatic necrosis and sinusoidal leukocytosis (H&E, ×20). (**F**) Kidney of a hamster of the injected group showing marked vacuolar degeneration and necrosis of tubular epithelium associated with thickening of the tubular and glomerular basement membranes, swelling of glomerular tuft, congestion of intertubular blood vessels, and intertubular hemorrhage (H&E, ×40).

Figure 3 Kidneys of hamsters of the injected group.
Notes: (**A**) Kidney of a hamster of the injected group showing marked vacuolar degeneration and necrosis of tubular epithelium together with an increased mesangial matrix and hyalinization of glomerular tuft and tubular basement membrane (hematoxylin and eosin stain [H&E], magnification, ×40). (**B**) Kidney of a hamster of the injected group showing focal interstitial mononuclear cell infiltration (H&E, ×40).

epithelium associated with thickening of the tubular and glomerular basement membranes, congestion of intertubular blood vessels, and intertubular hemorrhage (Figure 2F). Intraluminal casts of proteinaceous materials were commonly observed. Marked vacuolar degeneration and necrosis of tubular epithelium together with an increased mesangial matrix and hyalinization of glomerular tuft and tubular basement membrane were observed in two cases (Figure 3A). Multifocal areas of monolymphocytic interstitial cell infiltrates were commonly observed in most cases (Figure 3B).

Scoring system

Semiquantitative scoring showed that the overall lesions in the livers and kidneys did not exceed the moderate changes (Tables 2–5 and Figures 4 and 5).

Discussion

Nanotechnology has recently emerged as a promising approach in the diagnosis and treatment of a variety of diseases. GNPs have been suggested as an auxiliary tool in eradicating tumors in the context of photothermal therapy.[10] However, the translation of such techniques into comprehensive therapeutic modalities is still pending. One reason is that the safety issues of GNPs and the questions over their

Table 2 Scoring of histopathological lesions in the liver of 18 nm GNP-injected hamsters

Lesion description	Control	Gold-treated animals									
Liver		1	2	3	4	5	6	7	8	9	10
Cytoplasmic vacuolation	0	1	1	3	3	2	3	1	2	2	3
Vascular congestion	0	0	1	3	2	2	3	2	2	1	3
Perivascular and portal cell infiltration	0	0	2	3	3	1	3	1	2	1	2
Focal hepatic necrosis	0	0	1	3	2	1	2	1	2	0	3
Paracentral necrosis	0	0	0	1	0	0	1	0	0	0	0
Sinusoidal dilatation and leukocytosis	0	0	0	2	0	0	1	0	0	0	0

Notes: 0, none; 1, mild; 2, moderate; 3, severe.
Abbreviation: GNP, gold nanoparticle.

metabolic fate are still unresolved and need further investigations at a preclinical level.[6,43]

Our study was done on Syrian golden hamsters. We are using these small animals to model the treatment of tumors of the upper aerodigestive tract by gold nanophotothermolysis. We detected several hematologic changes and some histopathological changes in the microscopic pictures of the liver and kidneys after I/P injection with 18 nm GNPs.

The erythrogram indicated the presence of macrocytosis and hypochromasia (high mean corpuscular volume and low mean cell hemoglobin concentration) in the RBCs of 18 nm GNP-injected hamsters. This is consistent with a previous study done by Zhang et al[12] and might be attributed to the ability of the 18 nm GNPs to cross the fenestrated endothelial membrane of the bone marrow (50–100 nm),[44,45] thus interfering with the normal erythropoiesis resulting in immature RBCs. Since Lasagna-Reeves et al[46] and Simpson et al[13] reported that GNPs <5 nm in diameter have no effect on RBCs' count and morphology, disagreement with our results may be attributed to different doses and duration of

Table 3 Scoring of histopathological lesions in the kidney of 18 nm GNP-injected hamsters

Lesion description	Control	Gold-treated animals									
Kidney		1	2	3	4	5	6	7	8	9	10
Cytoplasmic vacuolation of tubular epithelium	0	2	2	3	2	2	3	2	1	2	1
Tubular cell necrosis	0	2	2	3	1	1	2	1	1	2	1
Thickening of tubular and glomerular basement membrane	0	0	1	2	1	1	1	0	1	1	0
Hyalinization of glomerular tuft	0	0	0	2	0	0	1	0	0	0	0
Tubular casts	0	1	1	2	1	1	2	1	1	0	0
Hemorrhage	0	0	0	2	1	0	0	0	1	1	0
Vascular congestion	0	1	1	2	1	1	1	1	1	2	1
Interstitial cell infiltration	0	0	1	3	1	1	2	1	1	2	0

Notes: 0, none; 1, mild; 2, moderate; 3, severe.
Abbreviation: GNP, gold nanoparticle.

Table 4 Mean ± SD scores of lesions in livers of 18 nm GNPs-injected hamsters

Liver	Control	Gold-treated animal
Cytoplasmic vacuolation	0±0	2.1±0.26
Vascular congestion	0±0	1.9±0.31
Perivascular and portal cell infiltration	0±0	1.8±0.33
Focal hepatic necrosis	0±0	1.5±0.34
Paracentral necrosis	0±0	0.2±0.13
Sinusoidal dilatation and leukocytosis	0±0	0.3±0.21

Abbreviation: GNPs, gold nanoparticles.

Figure 4 Scoring of hepatic histopathological lesions after I/P injection of 18 nm GNPs in Syrian golden hamsters for 14 consecutive days.
Abbreviations: GNPs, gold nanoparticles; I/P, intraperitoneal.

exposure to GNPs and more importantly to different sizes of GNPs.

The leukocytosis observed in GNP-injected hamsters is in agreement with Simpson et al,[22] Zhang et al,[47] and Sengupta et al.[48] The elevation in total leukocytic count might be attributed to the immunogenic effect of GNPs[15] or to their ability to trigger an inflammatory response by stimulating the release of cytokines.[49] Previously reported leukocytosis after injection of 10 nm and 60 nm particles in mice was attributed to an inflammatory response.[50] The monocytosis in the 18 nm GNP-injected hamsters can be regarded as an immune response attributed to the role of monocytes in the removal of xenobiotics, such as GNPs, from the circulation.[27]
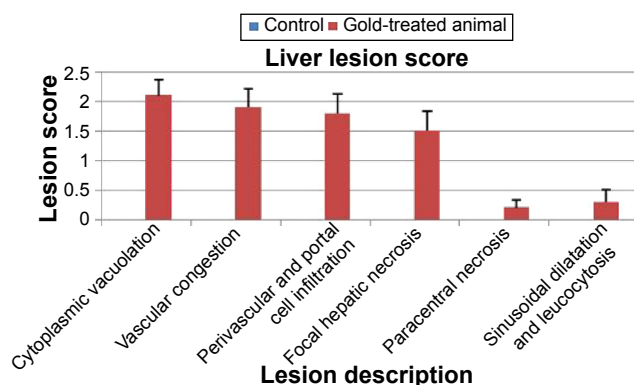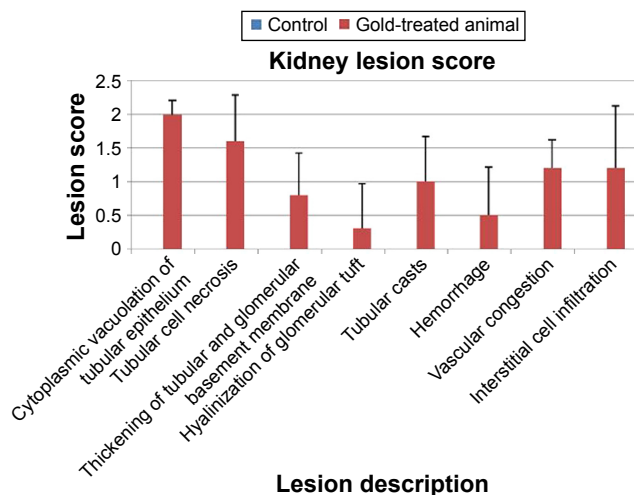
The lack of significant changes in the hepatic and renal function tests is in agreement with many reports[14,46,48,51] and in contradiction with others.[15,47] In these latter reports, different routes of administration and different doses and sizes of GNPs were applied.

Eighteen-nanometer GNPs were accumulated in significant amounts in the liver and spleen and to lesser degrees in the lungs, kidneys, and heart following the I/P injection.

These results are consistent with a previous report by Lipka et al.[20] Although the spleen was proved to be the dominant target organ for the 30 nm particles,[50] we found that the primary target for the 18 nm GNPs was the liver, and we did not find any remarkable histopathological alterations in the spleens of the 18 nm GNP-injected hamsters.

The microscopic lesions shown in the hepatic and renal tissues of hamsters exposed to GNPs are in agreement with Terentyuk et al[52] and Das et al.[15] Hepatocytes' degeneration and necrosis might be attributed to an enhanced defense mechanism against foreign particles, intoxication, hemodynamic changes, or alteration in inflammation and apoptosis-related genes. The determination of the exact cause needs further studies.

The presence of vacuolar degeneration in the renal tissue might be attributed to increased intracellular water due to disturbed ions and fluid homeostasis. Other renal lesions

Table 5 Mean ± SD scores of lesions in kidneys of 18 nm GNPs-injected hamsters

Kidney	Control	Gold-treated animal
Cytoplasmic vacuolation of tubular epithelium	0±0	2±0.21
Tubular cell necrosis	0±0	1.6±0.69
Thickening of tubular and glomerular basement membrane	0±0	0.8±0.63
Hyalinization of glomerular tuft	0±0	0.3±0.67
Tubular casts	0±0	1±0.67
Hemorrhage	0±0	0.5±0.71
Vascular congestion	0±0	1.2±0.42
Interstitial cell infiltration	0±0	1.2±0.49

Abbreviation: GNPs, gold nanoparticles.

Figure 5 Scoring of renal histopathological lesions after I/P injection of 18 nm GNPs in Syrian golden hamsters for 14 consecutive days.
Abbreviations: GNPs, gold nanoparticles; I/P, intraperitoneal.

can be attributed to the toxic effects of GNPs during clearance by renal tissue.

Conclusion

The repeated administration of 30 ppb of 18 nm GNPs for 14 consecutive days in hamsters induced macrocytosis, hypochromasia, leukocytosis, neutrophilia, lymphocytosis, and monocytosis. I/P administration of 18 nm GNPs in hamsters had no effect on plasma proteins, liver, and renal function tests. However, some hepatic and renal tissue alterations were observed ranging from mild to marked degeneration and necrosis of hepatocytes and tubular epithelium.

Acknowledgments

Disclosure

The authors report no conflicts of interest in this work.

References

1. Daniel MC, Astruc D. Gold nanoparticles: assembly, supramolecular chemistry, quantum-size-related properties, and applications toward biology, catalysis, and nanotechnology. *Chem Rev*. 2004;104:293–346.
2. Kim T, Lee K, Gong MS, Joo SW. Control of gold nanoparticle aggregates by manipulation of interparticle interaction. *Langmuir*. 2005;21: 9524–9528.
3. Huang W, Qian W, Jain PK, El-Sayed MA. The effect of plasmon field on the coherent lattice phonon oscillation in electron-beam fabricated gold nanoparticle pairs. *Nano Lett*. 2007;7:3227–3234.
4. Bao QY, Geng DD, Xue JW, et al. Glutathione-mediated drug release from Tiopronin-conjugated gold nanoparticles for acute liver injury therapy. *Int J Pharm*. 2013;446:112–118.
5. Conde J, Larguinho M, Cordeiro A, et al. Gold-nanobeacons for gene therapy: evaluation of genotoxicity, cell toxicity and proteome profiling analysis. *Nanotoxicology*. 2014;8:521–532.
6. Liu CC, Yeung CY, Chen PH, Yeh MK, Hou SY. Salmonella detection using 16S ribosomal DNA/RNA probe-gold nanoparticles and lateral flow immunoassay. *Food Chem*. 2013;141:2526–2532.
7. Murphy CJ, Gole AM, Stone JW, et al. Gold nanoparticles in biology: beyond toxicity to cellular imaging. *Acc Chem Res*. 2008;41:1721–1730.
8. Gong T, Olivo M, Dinish US, Goh D, Kong KV, Yong KT. Engineering bioconjugated gold nanospheres and gold nanorods as label-free plasmon scattering probes for ultrasensitive multiplex dark-field imaging of cancer cells. *J Biomed Nanotechnol*. 2013;9:985–991.
9. Zhang J, Li C, Zhang X, et al. In vivo tumor-targeted dual-modal fluorescence/CT imaging using a nanoprobe co-loaded with an aggregation-induced emission dye and gold nanoparticles. *Biomaterials*. 2015;42:103–111.
10. El-Sayed IH, Huang X, El-Sayed MA. Selective laser photo-thermal therapy of epithelial carcinoma using anti-EGFR antibody conjugated gold nanoparticles. *Cancer Lett*. 2006;239:129–135.
11. Lin J, Wang S, Huang P, et al. Photosensitizer-loaded gold vesicles with strong plasmonic coupling effect for imaging-guided photothermal/ photodynamic therapy. *ACS Nano*. 2013;7:5320–5329.
12. Zhang XD, Wu HY, Wu D, et al. Toxicologic effects of gold nanoparticles in vivo by different administration routes. *Int J Nanomedicine*. 2010;5:771–781.
13. Simpson CA, Agrawal AC, Balinski A, Harkness KM, Cliffel DE. Short-chain PEG mixed monolayer protected gold clusters increase clearance and red blood cell counts. *ACS Nano*. 2011;5:3577–3584.
14. Sung JH, Ji JH, Park JD, et al. Subchronic inhalation toxicity of gold nanoparticles. *Part Fibre Toxicol*. 2011;8:16.
15. Das S, Debnath N, Mitra S, Datta A, Goswami A. Comparative analysis of stability and toxicity profile of three differently capped gold nanoparticles for biomedical usage. *Biometals*. 2012;25:1009–1022.
16. Chen YS, Hung YC, Liau I, Huang GS. Assessment of the in vivo toxicity of gold nanoparticles. *Nanoscale Res Lett*. 2009;4:858–864.
17. Cho WS, Cho M, Jeong J, et al. Size-dependent tissue kinetics of PEG-coated gold nanoparticles. *Toxicol Appl Pharmacol*. 2010;245: 116–123.
18. Tedesco S, Doyle H, Blasco J, Redmond G, Sheehan D. Oxidative stress and toxicity of gold nanoparticles in *Mytilus edulis*. *Aquat Toxicol*. 2010;100:178–186.
19. Abdelhalim MA. Gold nanoparticles administration induces disarray of heart muscle, hemorrhagic, chronic inflammatory cells infiltrated by small lymphocytes, cytoplasmic vacuolization and congested and dilated blood vessels. *Lipids Health Dis*. 2011;10:233.
20. Lipka J, Semmler-Behnke M, Sperling RA, et al. Biodistribution of PEG-modified gold nanoparticles following intratracheal instillation and intravenous injection. *Biomaterials*. 2010;31:6574–6581.
21. Niidome T, Yamagata M, Okamoto Y, et al. PEG-modified gold nanorods with a stealth character for in vivo applications. *J Control Release*. 2006;114:343–347.
22. Simpson CA, Huffman BJ, Gerdon AE, Cliffel DE. Unexpected toxicity of monolayer protected gold clusters eliminated by PEG-thiol place exchange reactions. *Chem Res Toxicol*. 2010;23:1608–1616.
23. Girgis E, Khalil WK, Emam AN, Mohamed MB, Rao KV. Nanotoxicity of gold and gold-cobalt nanoalloy. *Chem Res Toxicol*. 2012;25:1086–1098.
24. Simpson CA, Salleng KJ, Cliffel DE, Feldheim DL. In vivo toxicity, biodistribution, and clearance of glutathione-coated gold nanoparticles. *Nanomedicine*. 2013;9:257–263.
25. Kim JH, Kim JH, Kim KW, Kim MH, Yu YS. Intravenously administered gold nanoparticles pass through the blood-retinal barrier depending on the particle size, and induce no retinal toxicity. *Nanotechnology*. 2009;20:505101.
26. Hillyer JF, Albrecht RM. Gastrointestinal persorption and tissue distribution of differently sized colloidal gold nanoparticles. *J Pharm Sci*. 2001;90:1927–1936.
27. Schleh C, Semmler-Behnke M, Lipka J, et al. Size and surface charge of gold nanoparticles determine absorption across intestinal barriers and accumulation in secondary target organs after oral administration. *Nanotoxicology*. 2012;6:36–46.
28. Hirn S, Semmler-Behnke M, Schleh C, et al. Particle size-dependent and surface charge-dependent biodistribution of gold nanoparticles after intravenous administration. *Eur J Pharm Biopharm*. 2011;77:407–416.
29. Vairaktaris E, Spyridonidou S, Papakosta V, et al. The hamster model of sequential oral oncogenesis. *Oral Oncol*. 2008;44:315–324.
30. Estensen RD, Anderson WR, Galbraith AR, et al. A method of producing carcinoma in upper aerodigestive tree and esophagus of the Syrian golden hamster using wounding and instillation of N-methylnitrosourea. *Cancer Epidemiol Biomarkers Prev*. 2007;16:1644–1650.
31. Frens G. Controlled nucleation for the regulation of particle size in monodisperse gold suspension. *Nat Phys Sci*. 1973;241:20–22.
32. Feldman BV, Zinkl JG, Jian NC. *Schalm's Veterinary Hematology*. Philadelphia: Lea and Fibiger; 2000.
33. Weichselbaum TE. An accurate rapid method for determination of protein in small amounts of blood, serum and plasma. *Am J Clin Pathol*. 1946;7:40.
34. Dumas BT, Biggs HG. *Standard Methods of Clinical Chemistry*. New York: Academic Press; 1972.
35. Reitman S, Frankel S. A colorimetric method for the determination of serum GOT and GPT. *Am J Clin Pathol*. 1957;28:53–63.

36. Searcy RL, Reardon JE, Foreman JA. Estimation of urea. *Am J Med Technol*. 1967;33:15–20.

37. Fabiny DL, Ertingshausen G. Automated reaction-rate method for determination of serum creatinine. *Clin Chem*. 1971;17:696–700.

38. Kehoe DF, Sullivan DM, Smith RL. Determination of gold in animal tissue by graphite furnace atomic absorption spectrophotometry. *J Assoc Off Anal Chem*. 1988;71:1153–1155.

39. Bancroft DJ, Cook CH, Stirling RW, Turner DR. *Manual of Histopathological Techniques and Their Diagnostic Applications*. Edinburgh: Churchill Livingston; 1994.

40. Standardized System of Nomenclature and Diagnostic Criteria (SSNDC) Guides [webpage on the Internet]. Society of Toxicologic Pathology. Available from: http://www.toxpath.org/ssndc.asp. Accessed September 17, 2015.

41. Mann PC, Vahle J, Keenan CM, et al. International harmonization of toxicologic pathology nomenclature: an overview and review of basic principles. *Toxicol Pathol*. 2012;40:7S–13S.

42. Duncan DB. Multiple range and multiple F tests. *Biometrics*. 1955; 11:1–42.

43. Caruthers SD, Wickline SA, Lanza GM. Nanotechnological applications in medicine. *Curr Opin Biotechnol*. 2007;18:26–30.

44. Porter CJ, Moghimi SM, Illum L, Davis SS. The polyoxyethylene/polyoxypropylene block co-polymer poloxamer-407 selectively redirects intravenously injected microspheres to sinusoidal endothelial cells of rabbit bone marrow. *FEBS Lett*. 1992;305:62–66.

45. Alexis F, Pridgen E, Molnar LK, Farokhzad OC. Factors affecting the clearance and biodistribution of polymeric nanoparticles. *Mol Pharm*. 2008;5:505–515.

46. Lasagna-Reeves C, Gonzalez-Romero D, Barria MA, et al. Bioaccumulation and toxicity of gold nanoparticles after repeated administration in mice. *Biochem Biophys Res Commun*. 2010;393:649–655.

47. Zhang XD, Wu D, Shen X, Liu PX, Fan FY, Fan SJ. In vivo renal clearance, biodistribution, toxicity of gold nanoclusters. *Biomaterials*. 2012; 33:4628–4638.

48. Sengupta J, Datta P, Patra HK, Dasgupta AK, Gomes A. In vivo interaction of gold nanoparticles after acute and chronic exposures in experimental animal models. *J Nanosci Nanotechnol*. 2013;13:1660–1670.

49. Dwivedi PD, Tripathi A, Ansari KM, Shanker R, Das M. Impact of nanoparticles on the immune system. *J Biomed Nanotechnol*. 2011;7: 193–194.

50. Zhang XD, Wu D, Shen X, et al. Size-dependent in vivo toxicity of PEG-coated gold nanoparticles. *Int J Nanomedicine*. 2011;6:2071–2081.

51. Huang XL, Zhang B, Ren L, et al. In vivo toxic studies and biodistribution of near infrared sensitive Au-Au(2)S nanoparticles as potential drug delivery carriers. *J Mater Sci Mater Med*. 2008;19:2581–2588.

52. Terentyuk GS, Maslyakova GN, Suleymanova LV, et al. Circulation and distribution of gold nanoparticles and induced alterations of tissue morphology at intravenous particle delivery. *J Biophotonics*. 2009;2: 292–302.